





Article

Impact of SWMM Fouling and Position on the Performance of SWRO Systems in Operating Conditions of Minimum SEC

Alejandro Ruiz-García ^{1,*} , Mudhar A. Al-Obaidi ² , Ignacio Nuez ¹  and Iqbal M. Mujtaba ³ 

¹ Department of Electronic Engineering and Automation, University of Las Palmas de Gran Canaria, Campus Universitario de Tafira, 35017 Las Palmas de Gran Canaria, Spain; ignacio.nuez@ulpgc.es

² Department of Computer Techniques, Technical Institute of Baquba, Middle Technical University, Baquba 00964, Iraq; dr.mudhar.alaubedy@mtu.edu.iq

³ Department of Chemical Engineering, Faculty of Engineering and Informatics, University of Bradford, Bradford BD7 1DP, UK; i.m.mujtaba@bradford.ac.uk

* Correspondence: alejandro.ruiz@ulpgc.es

Abstract: Due to water stress in the world in general desalination technologies are becoming increasingly important. Among the available technologies, reverse osmosis (RO) is the most widespread due to its reliability and efficiency compared to other technologies. The main weakness of RO is the loss of performance due to membrane fouling, which usually affects the water permeability coefficient (A), causing it to decrease. In RO desalination plants, fouling does not affect all spiral wound membrane modules (SWMMs) in the pressure vessels (PVs) in the same way. This will depend on the type of fouling and the position of the SWMM inside the PV. In this study, the impact of A and the position of the SWMM on the performance of the RO system is analyzed. For this purpose, decrements of up to 50% have been assumed for the seven SWMMs in series considering nine commercial SWMM models. The operating point analyzed is that which minimizes the specific energy consumption (SEC), a point obtained in a previous work carried out by the authors. The results show how the impact of A on the SWMM in the first position is more significant than the impact on modules that are in another position for the nine SWRO models studied. A drop of 50% in the coefficient A of the first element produces a permeate loss in the pressure pipe between 0.67 and 1.35 m³ d⁻¹. Furthermore, it was observed that the models with the lowest coefficient A exhibited the highest performance losses in terms of permeate production when A was decreased.

Keywords: desalination; reverse osmosis; membranes; fouling; energy consumption; simulation



Citation: Ruiz-García, A.; Al-Obaidi, M.A.; Nuez, I.; Mujtaba, I.M. Impact of SWMM Fouling and Position on the Performance of SWRO Systems in Operating Conditions of Minimum SEC. *Membranes* **2023**, *13*, 676. <https://doi.org/10.3390/membranes13070676>

Academic Editors: Hsueh-Chia Chang and Hongjun Lin

Received: 15 May 2023
Revised: 2 July 2023
Accepted: 16 July 2023
Published: 18 July 2023



Copyright: © 2023 by the authors. Licensee MDPI, Basel, Switzerland. This article is an open access article distributed under the terms and conditions of the Creative Commons Attribution (CC BY) license (<https://creativecommons.org/licenses/by/4.0/>).

1. Introduction

The shortage of water suitable for human consumption and other activities has been at least partially remedied by desalination for several decades [1]. Among the technologies available on a large scale to desalinate both seawater and brackish water [2], the most widespread is reverse osmosis (RO) [3,4]. This is due to its better energy efficiency compared to other technologies [5,6]. Climate change causes a rise in global temperatures, which leads to increased water stress [7]. This will drive the installation of desalination plants where they were not necessary just a few years ago. New technologies continue to be studied to efficiently desalinate seawater and brackish water. These include forward osmosis [8,9], pressure-retarded osmosis [10,11], osmotic distillation [12] and thermo-osmosis [13]. However, RO remains the most widespread technology [14]. Although the RO process is more efficient than others from the perspective of energy consumption, it is still a relatively intensive process regarding the energy required due to certain limitations [15]. It is crucial to investigate how to make this process more efficient through the development of, for example, more efficient and fouling-resistant membranes [16,17], improved energy recovery devices (ERDs) [18,19], enhanced automation and control [20],

optimal RO system design [21] and the determination of optimal operating points to reduce the energy required [22–24].

1.1. Optimization of RO Systems

Many studies have been conducted in relation to the optimization of RO systems and the impact of fouling on their efficiency [25–27]. Regarding the optimization of RO system design and operation, Lu et al. [28] explored the optimal design of seawater (SWRO) and brackish water (BWRO) systems using different spiral wound membrane modules (SWMMs) and considered the use of ERDs and different stages to minimize total annualized costs. Vince et al. [29] carried out a multi-objective optimization of BWRO desalination plants, while Li [30,31] used constrained nonlinear optimization to minimize specific energy consumption (SEC) in RO systems. Du et al. [32] proposed an optimization method for BWRO and SWRO desalination plants with SWMMs and later [33,34] carried out further studies on optimization methods considering different RO system designs. Li and Noh [35] validated a model used for optimization of the operation of a BWRO desalination plant. Jiang et al. [36] studied the optimal operation of a full-scale SWRO desalination plant with four storage tanks, while Du et al. [37] explored the optimization of SWRO systems for boron removal. The studies considered different factors, including feedwater concentration, membrane modules, stages, ERDs, inter-stage pumps, and water recovery rates. Constraints, such as permeate quality, were also taken into account.

Kotb et al. [38] conducted an intriguing research study that evaluated the optimization of SWRO process configurations and operating conditions. They assessed systems with various stages and retentate bypass. They also took into consideration ERDs and finally recommended that permeate flows of between $144 \text{ m}^3 \text{ d}^{-1}$ and $288 \text{ m}^3 \text{ d}^{-1}$ were suitable for RO systems with one and two stages, respectively, to minimize production costs. Ahunbay et al. [39] investigated the minimization of the SEC of SWRO systems using a multi-stage arrangement comprising nanofiltration SWMMs, achieving flow recovery (R) rates of about 65%. Alsarayreh et al. [40] aimed to minimize and assess the SEC of an existing BWRO desalination plant by changing the operating conditions and incorporating an ERD, obtaining reductions in the range of 47–53.8% compared to the original design without the ERD. Kim et al. [41] optimized SWRO systems with two stages and SW400R SWMMs from LG Chem, considering ERDs and focusing on energy efficiency. Chu et al. [42] conducted a study to determine the optimal design and operating conditions of a full-scale SWRO desalination plant with two trains, both with ERD and a second pass with BWRO SWMMs. In both studies, they used the manufacturer's software (CSMPRO5, <https://www.csmfilter.com/csm/03result/Software.asp>, Toray, Tokyo, Japan) to evaluate the installation of 16-inch SWMMs from Toray and concluded that the optimal energy-efficient split partial ratio was 4.5:5.5, satisfying a final permeate concentration (C_p) requirement of 0.3 g L^{-1} or less and a normalized SEC of less than 0.1 kWh m^{-3} . The objective of another study by the same group [43] was to identify operational strategies that could lower the costs associated with running and maintaining BWRO desalination plants in South Korea. To this end, they examined the potential benefits of incorporating low pressure SWMMs and attained to a reduction in SEC of approximately 16%.

1.2. Fouling Impact on RO System Performance

Membrane fouling is perhaps the weakest point in RO processes [16,17]. Fouling can be organic [44,45], inorganic [46,47] and biological [48,49]. In terms of performance, fouling mainly has two types of impact. Firstly, it decreases the water permeability coefficient (A) of the membrane, which implies having to increase the feed pressure to maintain production, which translates in turn into an increase in SEC [50,51]. Secondly, it causes an increase in the solute permeability coefficient (B), which leads to an increase in the passage of salts through the membrane, which in turn can compromise the use of the permeate due to a worsening of its quality in terms of concentration [52]. An additional consequence is the increase in pressure drop across the membrane elements due to the deposition of fouling

agents on the membrane surface [52]. As the pressure drop increases, the efficiency of the process in terms of specific energy consumption also decreases.

The fouling impact on permeate flux (J_p) and therefore on A in long-term operation was studied by Wilf et al. [53]. The experimental data of three years of operation from different SWRO desalination plants were used. They observed decrements between 25 and 20% in the J_p of the entire RO system. Four years of operating data from a full-scale SWRO desalination plant were used by Mohamed et al. [54] to study performance decline due to fouling effects. The installed SWMM was the TFC 2822 Fluid system™, the initial feed pressure (p_f) was 67 bar and the flux recovery R ranged between 26–33%. A 44% reduction in terms of J_p was observed. Abbas et al. [55] studied the performance decline of the SWMM BW30-400 Filmtec™ in a full-scale BWRO desalination plant with data obtained from five years of operation. It was found that over an operating period of 500 days, the A for the overall plant decreased by about 25% and salt rejection dropped by 1.9%. Belkacem et al. [56] observed a performance decline of the SWMM BW30LE-440 Filmtec™ in a BWRO desalination plant with two stages and with re-circulation. A 10% performance decline in 20 weeks of operation in terms of J_p was seen. Fouling results in changes to the operating conditions in RO desalination plants to maintain permeate production, modifying the optimal operating points. Sassi and Mujtaba [57] optimized an existing BWRO system with three stages taking into consideration the effect of fouling on performance in a simulation-based study. They determined a 20% in savings in terms of SEC compared to the base case. Park et al. [58] carried out a simulation-based study of a full-scale SWRO system for boron removal considering fouling. The fouling effect was applied through the mass transfer coefficient (k) as fouling enhances the concentration polarization, and so the resistance increase due to fouling was ignored. An increment of 0.78 kWh m^{-3} was obtained due to the fouling effect. A cost optimization study on the BWRO process considering fouling was done by Ang et al. [59]. Nanofiltration and BWRO SWMMs were considered in a quite short operating time during a laboratory-scale experiment. J_p decreased at an average 5% for all the membranes, which was attributed to fouling phenomena. Kim and Hong [60] optimized SWRO systems with an internally staged design method. A total of 36 combinations with three commercial SWMMs from LG Chem and pressure vessels (PVs) with 7 SWMMs in series were assessed. They found that the internally staged combinations were more effective in terms of SEC when the SWMMs were fouled under high R and flux conditions.

In RO systems, the SWMMs are arranged in series in PVs, and fouling does not affect all modules equally [61–63]. Usually, the fouling effect is measured for the entire RO system due to the distribution of available sensors, which are usually at the beginning and end of each stage. This does not allow for an evaluation of the impact of fouling inside the PV, and therefore also which SWMM is most affected by the fouling and is more susceptible to being replaced than others so that the performance of the RO desalination plant is not so affected.

The aim of this study is to evaluate the performance of an SWRO system with seven SWMMs in series and nine different models of commercial SWMMs, considering A reductions of individual elements as an estimate of the effect of fouling on these elements.

2. Materials and Methods

2.1. Commercial SWMMs

The characteristics of commercial SWRO SWMMs employed in this study are given in Table 1. The SWMMs used as well as the main characteristics in terms of membrane surface (S_m), feed channel height (h) and water and solute permeability coefficients A_0 and B are shown in Table 1. In order to make the results obtained in the simulations more realistic, we considered certain restrictions for different SWMMs that are usually recommended by the membrane manufacturers in terms of maximum feed flow (Q_f) ($384 \text{ m}^3 \text{ d}^{-1}$), maximum Q_p (33.36 and $36.24 \text{ m}^3 \text{ d}^{-1}$ for the SWMMs with S_m of 37.16 and 40.88 m^2 , respectively), minimum brine flow (Q_b) ($72 \text{ m}^3 \text{ d}^{-1}$) and maximum R (16%). For the nine SWMMs

considered, the same porosity in the feed-brine channel (ϵ) (0.89), friction factor (λ) and Sherwood number (Sh) were estimated, as characteristics of feed spacer geometries of the SWMMs are not supplied by the membrane manufacturers.

Table 1. S_m , h , Rej (NaCl), A_0 , and B of the SWMMs [64].

Number	SWMM Model	S_m (m ²)	h (m)	Rej (%)	A_0 (m Pa ⁻¹ s ⁻¹)	B (m s ⁻¹)
1	Toray RO TSW-LE-400	37.16	8.64×10^{-4}	99.69	8.75×10^{-12}	2.23×10^{-8}
2	Toray RO TM800V-440	40.88	7.11×10^{-4}	99.86	6.00×10^{-12}	1.45×10^{-8}
3	Toray RO TM800V-400	37.16	8.64×10^{-4}	99.86	6.08×10^{-12}	1.46×10^{-8}
4	Hydraunautics SWC6-LD-400	37.16	8.64×10^{-4}	99.69	8.44×10^{-12}	2.20×10^{-8}
5	Hydraunautics SWC4-MAX	40.88	7.11×10^{-4}	99.85	3.64×10^{-12}	1.17×10^{-8}
6	Hydraunautics SWC4-LD	37.16	8.64×10^{-4}	99.85	3.58×10^{-12}	1.17×10^{-8}
7	Filmtec™ SW30XLE-400	37.16	7.11×10^{-4}	99.86	6.06×10^{-12}	1.45×10^{-8}
8	Filmtec™ SW30HRLE-400	37.16	7.11×10^{-4}	99.85	3.75×10^{-12}	1.19×10^{-8}
9	Filmtec™ SW30XHR-440	40.88	7.11×10^{-4}	99.86	3.19×10^{-12}	9.86×10^{-9}

2.2. Equations and Simulation Algorithm for SWRO Systems

The equations used to estimate the SWRO system performance came from the solution-diffusion transport model [1,65], which is commonly used for simulating RO systems as it usually provides results close to the real behaviour of this process. The equations were applied considering averages per SWMM and in a sequential manner, with the outputs of the first SWMM used as the inputs of the second SWMM. For this study, only 1 PV with 7 SWMMs in series was considered (Figure 1), since for SWRO desalination plants with higher production capacity the results obtained would simply have to be multiplied by the number of PVs desired in the SWRO desalination plant. The variation of temperature T and pressure drop in the permeate side along the SWMMs and PV were disregarded. The algorithm used for the performance estimation of the SWRO system can be found in a previous study [21]. To determine all the above variables, the aforementioned algorithm was implemented in MATLAB® 2021b. The operating point that minimizes the energy consumption for each of the 9 SWMMs studied was considered for 7 SWMMs in series and $C_f = 30 \text{ g L}^{-1}$. These operating points were obtained in a previous study [64]. This means that p_f and Q_f are already established for each SWMM model, as shown in Table 2. In this study, decreases in the A coefficient from 10% to 50% were considered for each of the SWMMs in series and for each of the 9 SWMM models considered. That is, it was assumed that the first SWMM of the 7 in series suffers fouling such that it loses performance and the A coefficient is reduced while the rest of the SWMMs in series continue with the initial A_0 coefficient (new SWMM). Subsequently, the same approach is used with the second SWMM considering that the other 6 SWMMs have not been fouled, and so on up to the seventh element. This allows estimating the impact of SWMM fouling on the SWRO system performance even if the SWMMs are exchanged in position once they are affected by fouling in terms of reduction of the A coefficient. For this purpose, the transport equations shown in Table 3 were used. This study did not consider variations in coefficient B due to fouling. It should be noted that fouling can also cause the pressure drop to increase along the PV [66], which was also not considered in this study.

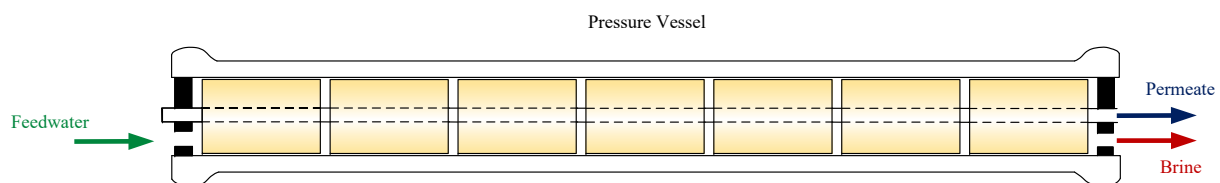


Figure 1. Flow diagram of the PV with 7 SWMMs in series.

Table 2. p_f , Q_f , R , C_p and p_b to obtain minimum SEC with $C_f = 30 \text{ g L}^{-1}$ and considering 7 SWMMs in series [64].

Parameter	SWMM Model								
	1	2	3	4	5	6	7	8	9
p_f (bar)	45.25	45.25	48.50	45.5	49.50	49.50	46.75	49.25	49.50
Q_f ($\text{m}^3 \text{ h}^{-1}$)	5.7	5.7	5.9	5.7	5.9	5.7	5.8	5.8	5.8
R (%)	47.16	46.96	49.12	47.35	49.1	47.36	48.06	48.21	48.2
C_p (mg L^{-1})	378.82	263.88	238.22	373.43	201.75	195.62	235.14	190.08	172.54
p_b (bar)	44.54	44.17	47.76	44.79	48.35	48.75	45.45	47.91	48.35
SEC (kWh m^{-3})	2.665	2.677	2.743	2.670	2.801	2.903	2.702	2.838	2.853

Table 3. Equations based on solution–diffusion transport phenomena in the SWRO process [64].

Permeate flow	$Q_p = A \cdot TMP \cdot S_m$	(1)
Water permeability coefficient	$A_i = A_0 \cdot TCF \cdot FF$	(2)
Temperature correction factor (If $T \geq 25 \text{ }^\circ\text{C}$)	$TCF = \exp\left[2640 \cdot \left(\frac{1}{298} - \frac{1}{273 + T}\right)\right]$	(3)
Temperature correction factor (If $T \leq 25 \text{ }^\circ\text{C}$)	$TCF = \exp\left[3020 \cdot \left(\frac{1}{298} - \frac{1}{273 + T}\right)\right]$	(4)
Transmembrane pressure	$TMP = (\Delta p - \Delta \pi) = p_f - \frac{\Delta p_{fb}}{2} - p_p - \pi_m + \pi_p$	(5)
Feed-brine pressure drop	$\Delta p_{fb} = \lambda \cdot L \cdot \frac{\rho_{fb} v_{fb}^2}{d_h} \frac{1}{2}$	(6)
Friction factor [67,68]	$\lambda = K_\lambda \cdot 6.23 Re^{-0.3}$	(7)
Reynolds number	$Re = \frac{\rho_{fb} \cdot v_{fb} \cdot d_h}{\eta}$	(8)
Hydraulic diameter	$d_h = \frac{4\epsilon}{\frac{2}{h} + (1 - \epsilon)\frac{8}{h}}$	(9)
Feed-brine solution density [33]	$\rho_{fb} = 498.4 \cdot M + \sqrt{248,400 + 752.4 \cdot C_{fb} \cdot M}$	(10)
Empirical parameter [33]	$M = 1.0069 - 2.757 \times 10^{-4} \cdot T_{fb}$	(11)
Feed-brine concentration	$C_{fb} = C_f \cdot \left(\frac{1 + \frac{C_b}{C_f}}{2}\right)$	(12)
Osmotic pressure	$\pi = 4.54047 \cdot \left(10^3 \cdot C / (M_s \cdot \rho)\right)^{0.987}$	(13)
Concentration on membrane surface	$C_m = C_{fb} \cdot PF$	(14)
Polarization factor	$PF_i = \frac{C_m}{C_{fb}} = e^{\frac{J_p}{k}}$	(15)
Sherwood number [68]	$Sh = 0.065 \cdot Re^{0.875} \cdot Sc^{0.25} = \frac{k \cdot d_h}{D_s}$	(16)

Table 3. *Cont.*

Schmidt number	$Sc = \frac{\eta}{\rho_{fb} \cdot D_s}$	(17)
Solute diffusivity	$D_s = (0.72598 + 0.023087T_{fb} + 0.00027657T_{fb}^2) \times 10^{-9}$	(18)
Permeate concentration	$C_p = B \cdot PF \cdot TCF \cdot \frac{S_m}{Q_p} \cdot \left(\frac{C_f \cdot (1 + CF)}{2} \right)$	(19)
Concentration factor	$CF = \frac{100 - R \cdot (1 - Rej)}{100 - R}$	(20)
Flux recovery	$R = 100 \cdot \frac{Q_p}{Q_f}$	(21)
Specific energy consumption	$SEC_i = \frac{P_{in_i}}{Q_{p_i}}$	(22)
Power input	$P_{in_i} = p_{f_i} Q_{f_i} \gamma_{f_i}$	(23)

The performance loss due to fouling was quantified through the flow factor (FF_i) which multiplies the coefficient A_0 of the SWMM in the position i (A_i). The temperature correction factor (TCF_i) was assumed to be 1 ($T_{fb_i} = 25$ °C for all SWMMs). TMP_i is the transmembrane pressure, Δp_i is the pressure gradient across the membrane, $\Delta\pi_i$ is the osmotic pressure gradient across the membrane, p_{p_i} is the permeate pressure (34,473.8 Pa for all SWMMs), π_{m_i} is the osmotic pressure on the membrane surface, π_{p_i} is the osmotic pressure in the permeate, L_i is the SWMM length (1 m for all SWMM models), v_{fb_i} is the feed-brine velocity, λ_i was multiplied by K_{λ_i} , a parameter established by Geraldes et al. [67] to take into consideration additional pressure losses in the feed side due to the SWMM fittings, PF_i is the polarization factor, k_{s_i} is the solute mass transfer coefficient and η_i is the dynamic viscosity of solution (8.91×10^{-4} kg m⁻¹ s⁻¹). The SEC was calculated considering the ideal performance (100% efficiency for the electrical engine and high pressure pump), which means that it was calculated with the power input (P_{in_i}) in the SWMMs.

3. Results and Discussion

Table 4 shows the results by SWMM model and position i for the operating points that minimize the SEC. The SWMMs with lower A_0 require more p_{f_i} , Q_{f_i} was quite similar for the 9 SWMMs considered, being between 5.7 and 5.9 m³ h⁻¹. In terms of p_{f_i} , it was observed how the largest pressure drops occur in the SWMMs with lower h_i (7.11×10^{-4}). The R_1 is lower for the SWMMs with lower A_0 , however the R_i drops are lower for the elements with lower A_0 and so permeate production is more uniform than for the SWMMs with higher A_0 . For all nine SWMMs considered, the PF_i decreases with increasing SWMM position. Despite the fact that v_{fb_i} decreases along the PV, causing PF_i to increase, its effect is outweighed by the reduction of Q_{p_i} along the PV in PF_i , resulting in an overall decrease in PF_i . In terms of SEC, the SWMMs became more energy inefficient as the position increased for the operating points considered. There may be operating points where this behavior changes. The SWMMs with lower A_0 were observed to have higher SEC_i in the first SWMM positions but lower in the last ones. This is due to the more uniform production for the SWMMs with lower A_0 . For SWMMs with higher A_0 , the later positions had lower Q_{p_i} implying overall higher SEC_i .

Table 4. p_{fi} , Q_{fi} , R_i , PF_i and SEC_i per SWMM model and position considering non-fouled SWMMs.

SWMM Model	Parameter	SWMM Position						
		1	2	3	4	5	6	7
1	p_{fi} (bar)	45.25	45.08	44.95	44.85	44.76	44.68	44.60
	Q_{fi} (m ³ h ⁻¹)	5.70	4.80	4.18	3.75	3.46	3.26	3.12
	R_i (%)	15.86	12.90	10.12	7.74	5.84	4.42	3.40
	PF_i	1.51	1.38	1.28	1.20	1.14	1.11	1.08
	SEC_i (kWh m ⁻³)	7.93	9.71	12.34	16.10	21.29	28.08	36.44
2	p_{fi} (bar)	45.25	44.99	44.80	44.64	44.50	44.38	44.27
	Q_{fi} (m ³ h ⁻¹)	5.70	4.80	4.17	3.74	3.45	3.26	3.12
	R_i (%)	15.86	13.07	10.25	7.73	5.70	4.17	3.09
	PF_i	1.40	1.30	1.22	1.16	1.11	1.08	1.06
	SEC_i (kWh m ⁻³)	7.93	9.56	12.14	16.04	21.69	29.56	39.80
3	p_{fi} (bar)	48.50	48.32	48.18	48.07	47.98	47.90	47.82
	Q_{fi} (m ³ h ⁻¹)	5.90	4.98	4.32	3.86	3.52	3.29	3.12
	R_i (%)	15.52	13.23	10.84	8.59	6.65	5.09	3.88
	PF_i	1.49	1.39	1.30	1.22	1.17	1.12	1.09
	SEC_i (kWh m ⁻³)	8.68	10.15	12.35	15.54	20.04	26.14	34.24
4	p_{fi} (bar)	45.50	45.33	45.20	45.10	45.00	44.93	44.86
	Q_{fi} (m ³ h ⁻¹)	5.70	4.80	4.18	3.75	3.46	3.25	3.11
	R_i (%)	15.84	12.94	10.19	7.81	5.91	4.47	3.44
	PF_i	1.50	1.38	1.28	1.20	1.15	1.11	1.08
	SEC_i (kWh m ⁻³)	7.98	9.73	12.32	16.04	21.15	27.92	36.22
5	p_{fi} (bar)	49.50	49.22	49.01	48.84	48.69	48.56	48.45
	Q_{fi} (m ³ h ⁻¹)	5.90	5.05	4.40	3.92	3.57	3.32	3.13
	R_i (%)	14.37	12.82	10.94	8.96	7.11	5.50	4.20
	PF_i	1.35	1.30	1.24	1.19	1.14	1.11	1.08
	SEC_i (kWh m ⁻³)	9.57	10.66	12.44	15.14	19.02	24.53	32.04
6	p_{fi} (bar)	49.50	49.33	49.19	49.07	48.98	48.89	48.82
	Q_{fi} (m ³ h ⁻¹)	5.70	4.97	4.39	3.94	3.60	3.34	3.15
	R_i (%)	12.87	11.66	10.21	8.66	7.17	5.81	4.64
	PF_i	1.39	1.34	1.28	1.23	1.18	1.14	1.11
	SEC_i (kWh m ⁻³)	10.68	11.75	13.38	15.74	18.98	23.37	29.23
7	p_{fi} (bar)	46.75	46.44	46.20	46.01	45.85	45.71	45.58
	Q_{fi} (m ³ h ⁻¹)	5.80	4.87	4.22	3.77	3.47	3.26	3.11
	R_i (%)	15.98	13.36	10.62	8.11	6.03	4.42	3.26
	PF_i	1.41	1.32	1.24	1.17	1.12	1.09	1.06
	SEC_i (kWh m ⁻³)	8.13	9.66	12.08	15.76	21.12	28.73	38.84
8	p_{fi} (bar)	49.25	48.93	48.68	48.48	48.31	48.16	48.03
	Q_{fi} (m ³ h ⁻¹)	5.80	5.00	4.38	3.91	3.57	3.32	3.14
	R_i (%)	13.80	12.38	10.64	8.80	7.04	5.49	4.23
	PF_i	1.34	1.29	1.24	1.19	1.14	1.11	1.08
	SEC_i (kWh m ⁻³)	9.91	10.98	12.71	15.30	19.06	24.37	31.54
9	p_{fi} (bar)	49.50	49.23	49.02	48.84	48.70	48.57	48.45
	Q_{fi} (m ³ h ⁻¹)	5.80	5.02	4.41	3.94	3.59	3.33	3.14
	R_i (%)	13.47	12.20	10.61	8.87	7.19	5.67	4.40
	PF_i	1.32	1.28	1.23	1.19	1.15	1.11	1.08
	SEC_i (kWh m ⁻³)	10.21	11.21	12.83	15.30	18.81	23.79	30.59

3.1. Implications of A_i Reduction on p_{fi}

Figure 2 shows the p_{fi} for each SWMM position, considering new membranes and a 50% reduction for the coefficient A_0 at position 1, for SWMM models 1 (Figure 2a) and 8 (Figure 2b). Both models have the same S_m , but model 1 has a higher A_0 coefficient than model 8 and a higher h (Table 1). This implies that v_{fb} will be lower for the SWMM in position 1, since this element will produce more permeate and the Q_{fb} will be lower

as well as having a higher h , so the pressure drop from one SWMM to the next will be lower, as shown in Figure 2. It should be noted that fouling would not only produce a decrease in A but also an increase in the pressure drop from one SWMM to another due to colloid deposition and organic fouling [66]. This effect would be expected to be most pronounced in SWMM 8 since it has a lower h . Overall, the pressure drop differences for each of the SWMM models did not show a representative difference between considering new SWMMs and reductions of 50% in the SWMM in first position. For SWMM model 1, the pressure drops along the PV were 0.65 and 0.67 bar considering, respectively, new SWMMs and the SWMM in position 1 with a decrease in A_0 of 50%, while for SWMM model 8 the corresponding values were 1.22 and 1.30 bar under the same conditions. It should be mentioned that similar expressions were used for λ (Equation (7)). If the membrane manufacturers were to provide these correlations, more accurate estimates could be obtained.

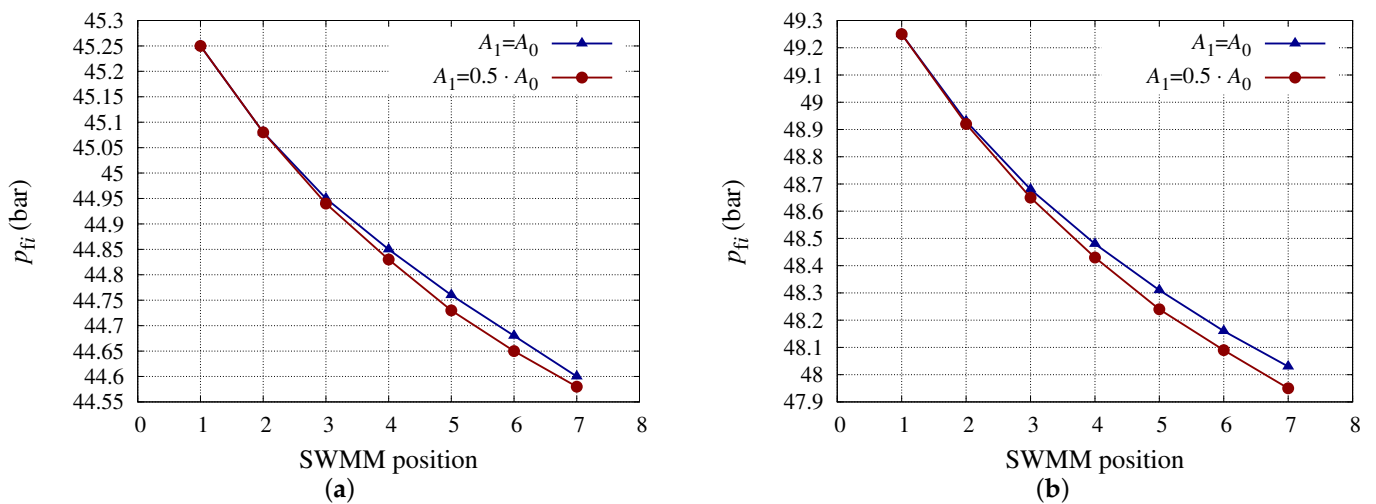


Figure 2. p_{fi} (bar) considering the SWMM in position 1 with different A_0 reductions. (a) p_{fi} (bar) for SWMM model 1 considering the SWMM in position 1 with different A_0 reductions. (b) p_{fi} (bar) for SWMM model 8 considering the SWMM in position 1 with different A_0 reductions.

3.2. Implications of A_i Reduction on R_i

Figure 3 shows the R_i for each SWMM position, considering new membranes and a 70% and 50% reduction for the coefficient A_0 at position 1, for SWMM models 4 (Figure 2a) and 6 (Figure 2b). Both models have the same S_m, h but different coefficient A_0 (Table 1), with this being higher for SWMM model 4 than for model 6. Both models show the same behavior in terms of R_i ; the more A_1 decreases the more R_1 decreases and the more R_i increases for SWMMs positioned further forward in the PV (positions 2 to 7). This is due to the fact that, for the PV input operating conditions, the lower π_{m_i} is the higher R_i is. This occurs because reducing the A_0 of the SWMM in the first position, which has the highest R (Table 4), causes Q_{fi} to increase for SWMMs in positions 2 to 7.

The decreases in A_i have repercussions on the R of the PV, and depending on the position of the fouled SWMM will have more or less an impact on R_i . The coefficient A_0 also plays an important role in the variations of R_i due to the decrease of the aforementioned coefficient. Tables 5 and 6 show, for SWMM models 2 and 9, respectively, the R of the PV, considering different decrements of A_0 for SWMMs located in different positions. In the operating points considered (Table 2), the SWMM in first position is the most relevant, which is why when the A_0 decrease affects the SWMM in that position it has a higher impact on the R_i of the PV, as can be seen in Tables 5 and 6. The SWMM models 2 and 9 have the same S_m and h . However, A_0 is higher for model 2 than model 9. The R_i drop for the A_i decrease conditions was higher for the SWMM with lower A_0 , in this case model 9, which means that, under fouling conditions, the RO system with this SWMM will experience

greater performance losses than SWMM model 1. However, the impact of fouling in terms of increased B coefficient, which would be more favorable for the SWMM model 9, was not evaluated. This could be critical when attention is paid to ions less rejected by SWRO membranes, such as boron and fluoride [69–71].

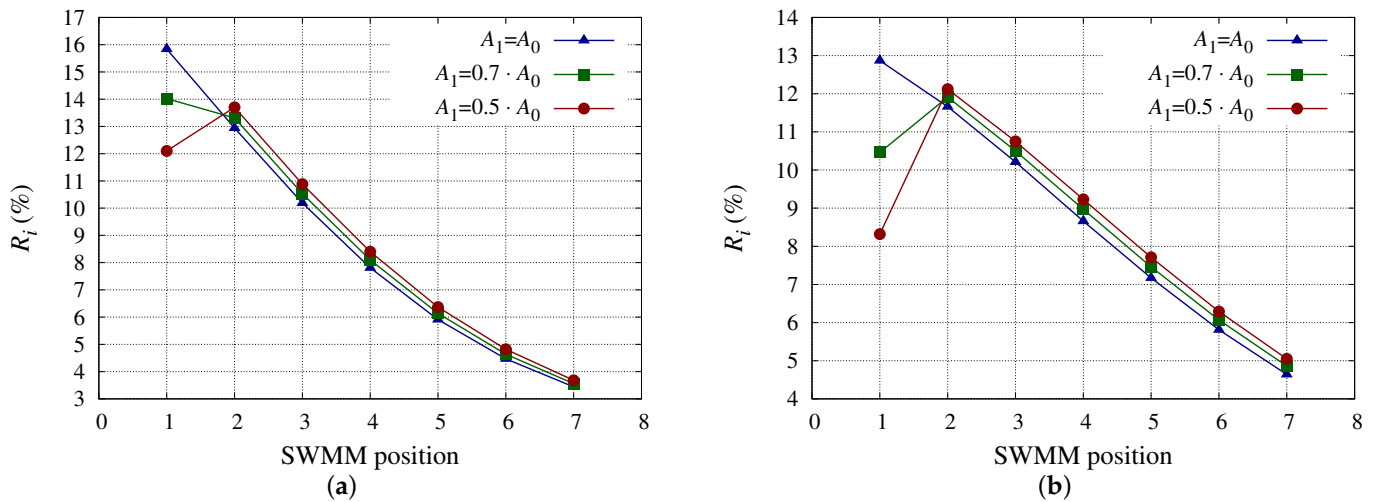


Figure 3. R_i (%) considering the SWMM in position 1 with different A_0 reductions. (a) R_i (%) for SWMM model 4 considering the SWMM in position 1 with different A_0 reductions. (b) R_i (%) for SWMM model 6 considering the SWMM in position 1 with different A_0 reductions.

Table 5. R (%) of the PV (7 SWMMs in series) with SWMM model 2 (Table 1) considering fouled SWMMs located in different positions.

Position of the Fouled SWMM	R (%) for SWMM Model 2				
	$A_i = 0.9A_0$	$A_i = 0.8A_0$	$A_i = 0.7A_0$	$A_i = 0.6A_0$	$A_i = 0.5A_0$
1	46.87	46.77	46.65	46.51	46.34
2	46.88	46.80	46.69	46.57	46.43
3	46.89	46.82	46.73	46.62	46.49
4	46.90	46.83	46.75	46.65	46.54
5	46.91	46.84	46.77	46.68	46.58
6	46.91	46.86	46.79	46.72	46.62
7	46.92	46.87	46.82	46.75	46.67

Table 6. R (%) of the PV (7 SWMMs in series) with SWMM model 9 (Table 1) considering fouled SWMMs located in different positions.

Position of the Fouled SWMM	R (%) for SWMM Model 2				
	$A_i = 0.9A_0$	$A_i = 0.8A_0$	$A_i = 0.7A_0$	$A_i = 0.6A_0$	$A_i = 0.5A_0$
1	48.03	47.86	47.66	47.44	47.19
2	48.05	47.89	47.71	47.51	47.28
3	48.07	47.92	47.76	47.57	47.35
4	48.08	47.95	47.79	47.62	47.42
5	48.09	47.96	47.82	47.66	47.47
6	48.10	47.98	47.85	47.69	47.51
7	48.10	47.99	47.87	47.73	47.56

3.3. Implications of A_i Reduction on PF_i

Figure 4 show the values of PF_i for SWMM models 3 (Figure 4a) and 5 (Figure 4b) considering different decrements of A_0 for each model. PF_i depends on J_p and k (Equation (15)).

The higher J_p is the higher PF_i is. High values of J_p are associated with high permeate production of the SWMM, making the following SWMM receive low Q_{f_i} which translates into low v_{fb_i} so that Re would also be low as well as k , resulting in high values of PF_i . The SWMM models 3 and 5 have different S_m , with the value being higher for model 5, while h and A_0 are higher for model 3. PF_i values for model 3 were higher than for model 5 due to its higher A_0 and despite having higher h . Because of the decrease in Q_{p_1} due to the decrease in A_1 , an increase in PF_i was observed in both SWMM models. The increase in PF_i in the last SWMM in the PV can bear a significant impact on the C_p .

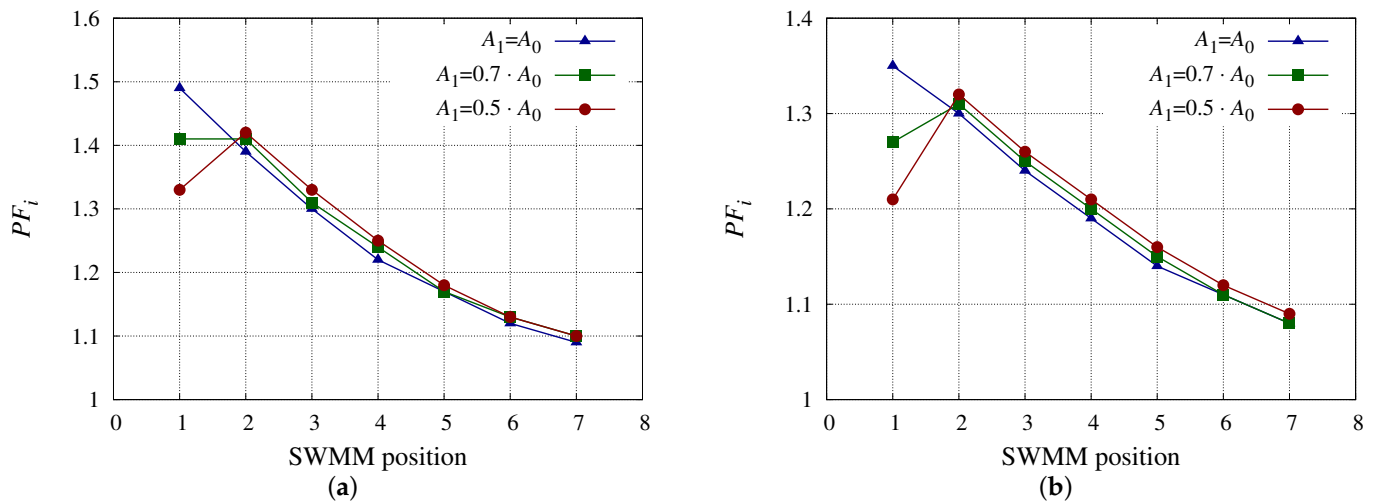


Figure 4. PF_i considering the SWMM in position 1 with different A_0 reductions. (a) PF_i for SWMM model 3 considering the SWMM in position 1 with different A_0 reductions. (b) PF_i for SWMM model 5 considering the SWMM in position 1 with different A_0 reductions.

Figure 5 shows the impact of the decrease in A_3 on PF_i for the SWMM models studied above. The effects are quite similar to the previous case (Figure 4) with the difference that the SWMM in position 1 has higher values in this case because A_1 has not decreased. Since A_1 has not decreased, the SWMM in second position has less Q_p , and so the PF_i is lower than in the previous case for both models (Figure 5a,b). As in the previous case, there is an increase of PF_i in the SWMMs positioned after the “fouled” one. It should be noted that the operating points considered, which minimize the SEC (Table 2), have quite low Q_{f_1} values. This results in a low cross-flow velocity profile and high PF_i values. Under fouling conditions (common in RO), it is not advisable to work in operating conditions with high PF_i since it promotes the deposition of fouling agents, whether colloidal, biofouling or even scaling, with the latter being common in BWRO where high values of R can be reached. Values of Q_{f_1} shown in Table 2 are below $6 \text{ m}^3 \text{ h}^{-1}$, while Q_{f_1} values above $7 \text{ m}^3 \text{ h}^{-1}$ are normally operated [52,53,55].

3.4. Implications of A_i Reduction on SEC_i

The impact on the SEC of the PV of the decrements considered for A_0 is quite low. In fact for SWMM model 1 (highest A_0 value) and new membranes the SEC is 2.665 kWh m^{-3} , and considering $A_1 = 0.5 \cdot A_0$ (which is the most unfavorable case studied) the value is 2.693 kWh m^{-3} . The aforementioned values for the SWMM model 9 (lowest A_0 value) are 2.853 and 2.913 kWh m^{-3} , respectively. In real RO desalination plants, fouling has a gradual impact on all SWMMs within the PV, causing decreases in A_0 to occur in them all. This would indeed considerably increase the SEC of the desalination plant, as can be seen in previously published studies [52,53,55]. Figure 6 shows the impact of the decrease in A_0 on SEC_i . It can be observed that the behaviour is similar for SWMM models 1 and 9. The decrease in A_1 translated into an increase in SEC_1 , but the following SWMMs experienced a SEC_i reduction. However, this reduction was not sufficient to balance the SEC_1 increase

produced in the SWMM in the first position in both SWMM models. The decrease in A_1 affected the SWMM model more with lower A_0 (model 9) in terms of SEC_i . This can be seen in Figure 6a,b, where the points and curves are farther apart for SWMM model 9 (Figure 6b) than for SWMM model 1 (Figure 6a).

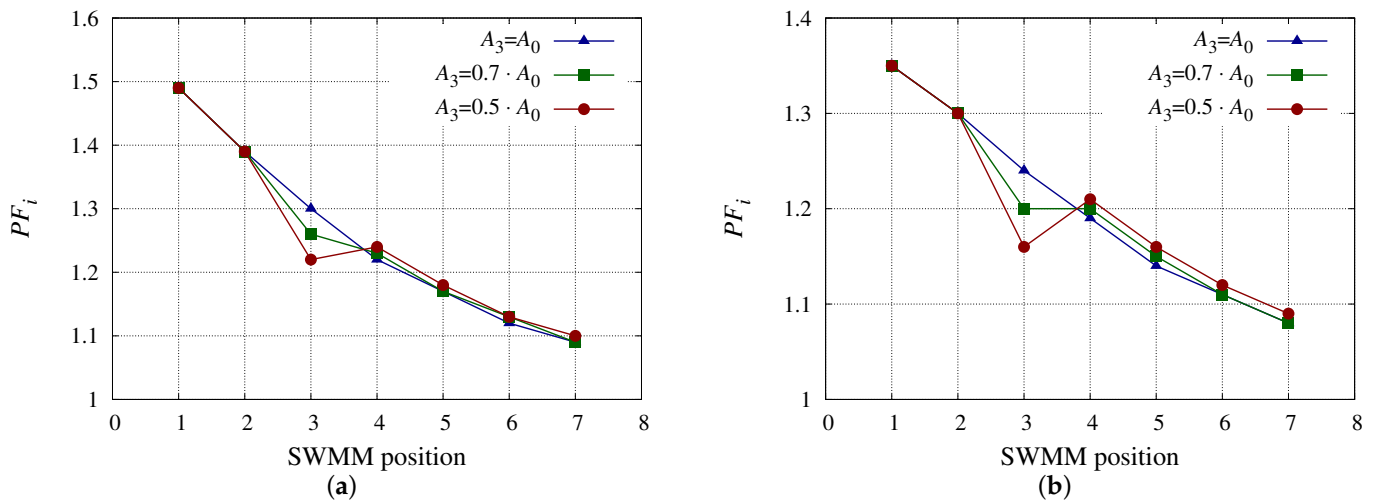


Figure 5. PF_i considering the SWMM in position 3 with different A_0 reductions. (a) PF_i for SWMM model 3 considering the SWMM in position 3 with different A_0 reductions. (b) PF_i for SWMM model 5 considering the SWMM in position 3 with different A_0 reductions.

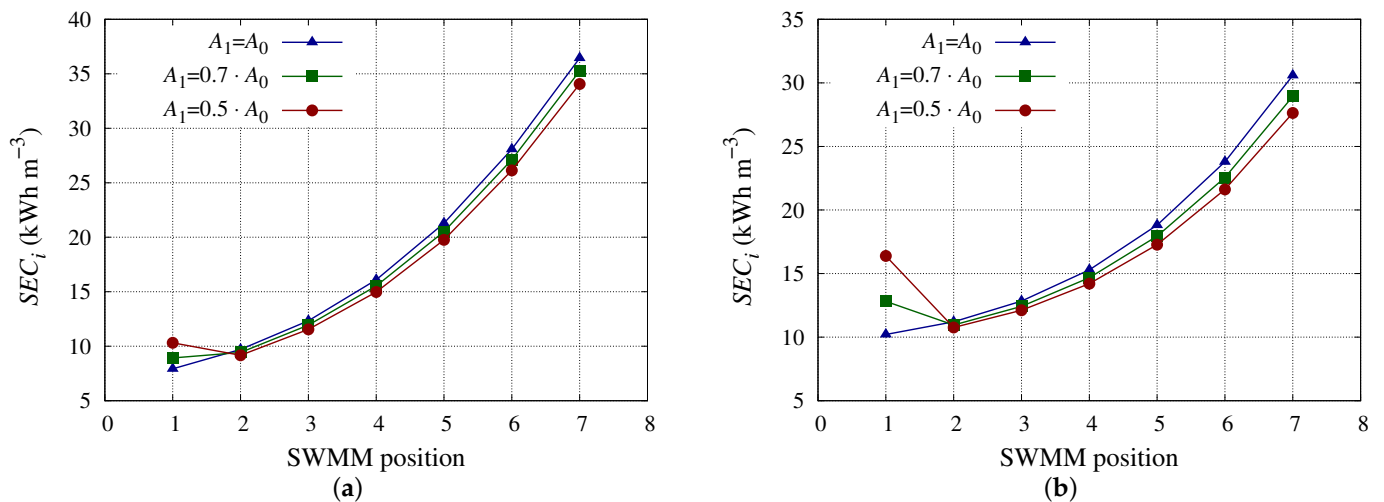


Figure 6. SEC_i considering the SWMM in position 1 with different A_0 reductions. (a) SEC_i for SWMM model 1 considering the SWMM in position 1 with different A_0 reductions. (b) SEC_i for SWMM model 9 considering the SWMM in position 1 with different A_0 reductions.

Figure 7 shows the impact of decreasing A_2 in terms of SEC_i . It shows the same trend as in Figure 6, but causing less impact on the SEC of the entire PV. In terms of SEC_i , in addition to other parameters, the decrease in A_1 had more impact than this decrease in subsequent SWMMs. In fact, considering decrements of 50% of A_i for SWMM model 9, the SEC for the entire PV was 2.913 kWh m⁻³ when the decrement was applied to A_1 , 2.908 kWh m⁻³ when it was applied to A_2 , 2.904 kWh m⁻³ when it was applied to A_3 , and so on to a value of 2.891 kWh m⁻³ when applied to the seventh SWMM. It should be noted that these results are conditioned by accounting for the operating points that minimize SEC in which the SWMM in position one is the most relevant. Under different operating

conditions where the highest R is not found in the SWMM in the first position, different results would be obtained.

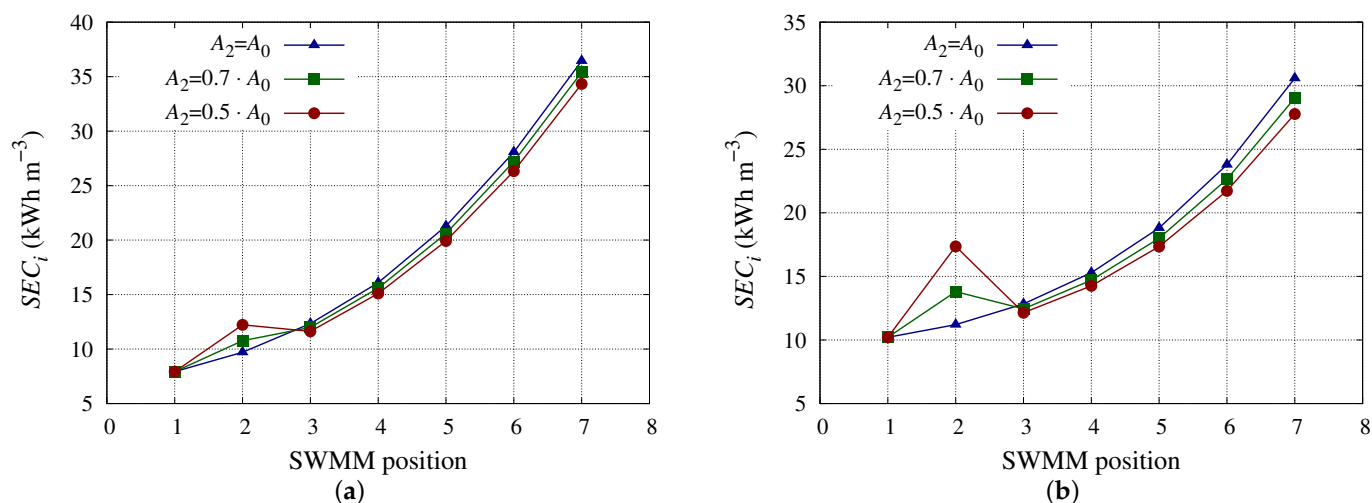


Figure 7. SEC_i considering the SWMM in position 2 with different A_0 reductions. (a) SEC_i for SWMM model 1 considering the SWMM in position 2 with different A_0 reductions. (b) SEC_i for SWMM model 9 considering the SWMM in position 2 with different A_0 reductions.

4. Conclusions

In this study, an evaluation was undertaken concerning how a decrease in the coefficient A of an SWMM at different positions within the PV affects the operating point that minimizes the SEC . For this purpose, a total of nine SWMM commercial models from three different membrane manufacturers were considered. At this operating point, the decrease in coefficient A_1 had the greatest impact on the performance of the PV, since this first SWMM produced the most permeate of all PVs for the nine SWMM models studied. When under operating conditions similar to those studied and when the first SWMM is subjected to fouling that produces decreases in the A coefficient, this should be the first SWMM to be replaced as it is the most relevant. This does not mean that, regardless of the operating conditions, this is always the case. This will depend on the nominal operating point of the plant. There may be, under other operating conditions, circumstances in which the most relevant SWMM is in a position other than first. As a future line of research, it is proposed to carry out this same study but for wide operating windows and to corroborate the results through experimental studies. In addition, a simultaneous decrease in A across various SWMMs should be also considered, as it would closer mimic the operation of real RO desalination plants. This, in turn, would help to determine which SWMMs are more critical allowing a more efficient SWMM replacement in the PV.

Author Contributions: Conceptualization, A.R.-G. and M.A.A.-O.; methodology, A.R.-G.; software, A.R.-G.; formal analysis, A.R.-G.; investigation, A.R.-G.; resources, A.R.-G. and I.N.; writing—original draft preparation, A.R.-G.; writing—review and editing, M.A.A.-O. and A.R.-G.; visualization, A.R.-G. and I.M.M.; supervision, I.M.M. and I.N.; funding acquisition, A.R.-G. and I.N. All authors have read and agreed to the published version of the manuscript.

Funding: This research was co-funded by the ERDF and the ACLIEMAC project grant number MAC2/3.5b/380 of the INTERREG V-A MAC 2014-2020 program.

Institutional Review Board Statement: Not applicable.

Informed Consent Statement: Not applicable.

Data Availability Statement: Not applicable.

Conflicts of Interest: The authors declare no conflict of interest.

Abbreviations

The following abbreviations are used in this manuscript:

Nomenclature

<i>A</i>	Water permeability coefficient ($\text{m Pa}^{-1} \text{s}^{-1}$)
<i>B</i>	Ion permeability coefficient (m s^{-1})
<i>C</i>	Concentration (g l^{-1})
<i>CF</i>	Concentration factor
<i>D</i>	Diffusivity ($\text{m}^2 \text{s}^{-1}$)
<i>d_h</i>	Hydraulic diameter (m)
<i>FF</i>	Flow factor
<i>h</i>	Feed spacer height
<i>J</i>	Flow per unit area ($\text{m}^3 \text{m}^{-2} \text{d}^{-1}$)
<i>K_λ</i>	Additional pressure losses factor
<i>k</i>	Mass transfer coefficient
<i>L</i>	Length of the spiral wound membrane module (m)
<i>m</i>	Molal concentration (mol kg^{-1})
<i>P_{in}</i>	Power input (kW)
<i>PF</i>	Polarization factor
<i>PV</i>	Pressure vessel
<i>p</i>	Pressure (Pa)
<i>Q</i>	Flow ($\text{m}^3 \text{s}^{-1}$)
<i>R</i>	Flow recovery (%)
<i>Re</i>	Reynolds number
<i>Rej</i>	Rejection (%)
<i>RO</i>	Reverse osmosis
<i>S_m</i>	Membrane surface (m^2)
<i>Sc</i>	Schmidt number
<i>SEC</i>	Specific energy consumption (kWh m^{-3})
<i>Sh</i>	Sherwood number
<i>SWMM</i>	Spiral wound membrane module
<i>T</i>	Temperature ($^{\circ}\text{C}$)
<i>TCF</i>	Temperature correction factor
<i>TMP</i>	Transmembrane pressure (Pa)
Greek letters	
ϵ	Porosity of the cross-sectional area in the feed channel
η	Dynamic viscosity ($\text{kg m}^{-1} \text{s}$)
γ	Specific weight (N m^{-3})
λ	Friction factor
ν	Velocity (m s^{-1})
π	Osmotic pressure (Pa)
ρ	Density (kg m^{-3})
Δp	Pressure gradient (Pa)
$\Delta\pi$	Osmotic pressure gradient (Pa)
Subscripts	
0	Initial
av	Average
f	Feed
fb	Feed-brine
<i>i</i>	Position of the SWMM within the PV
m	Membrane
p	Permeate
b	Brine
s	Solute

References

1. Qasim, M.; Badrelzaman, M.; Darwish, N.N.; Darwish, N.A.; Hilal, N. Reverse osmosis desalination: A state-of-the-art review. *Desalination* **2019**, *459*, 59–104. [[CrossRef](#)]
2. Honarparvar, S.; Zhang, X.; Chen, T.; Alborzi, A.; Afroz, K.; Reible, D. Frontiers of Membrane Desalination Processes for Brackish Water Treatment: A Review. *Membranes* **2021**, *11*, 246. [[CrossRef](#)] [[PubMed](#)]
3. Zapata-Sierra, A.; Cascajares, M.; Alcayde, A.; Manzano-Agugliaro, F. Worldwide research trends on desalination. *Desalination* **2021**, *519*, 115305. [[CrossRef](#)]
4. Kurihara, M. Current Status and Future Trend of Dominant Commercial Reverse Osmosis Membranes. *Membranes* **2021**, *11*, 906. [[CrossRef](#)] [[PubMed](#)]
5. Voutchkov, N. Energy use for membrane seawater desalination—Current status and trends. *Desalination* **2018**, *431*, 2–14. [[CrossRef](#)]
6. Nassrullah, H.; Anis, S.F.; Hashaikeh, R.; Hilal, N. Energy for desalination: A state-of-the-art review. *Desalination* **2020**, *491*, 114569. [[CrossRef](#)]
7. García-Rodríguez, L.; Delgado-Torres, A.M. Renewable Energy-Driven Desalination: New Trends and Future Prospects of Small Capacity Systems. *Processes* **2022**, *10*, 745. [[CrossRef](#)]
8. Giagnorio, M.; Morciano, M.; Zhang, W.; Hélix-Nielsen, C.; Fasano, M.; Tiraferri, A. Coupling of forward osmosis with desalination technologies: System-scale analysis at the water-energy nexus. *Desalination* **2022**, *543*, 116083. [[CrossRef](#)]
9. Jawad, J.; Hawari, A.H.; Zaidi, S.J. Modeling and Sensitivity Analysis of the Forward Osmosis Process to Predict Membrane Flux Using a Novel Combination of Neural Network and Response Surface Methodology Techniques. *Membranes* **2021**, *11*, 70. [[CrossRef](#)]
10. Ruiz-García, A.; Tadeo, F.; Nuez, I. Simulation tool for full-scale PRO systems using SWMMs. *Desalination* **2022**, *541*, 116025. [[CrossRef](#)]
11. Aumesquet-Carreto, M.; Ortega-Delgado, B.; García-Rodríguez, L. Opportunities of Reducing the Energy Consumption of Seawater Reverse Osmosis Desalination by Exploiting Salinity Gradients. *Membranes* **2022**, *12*, 1045. [[CrossRef](#)] [[PubMed](#)]
12. Lee, S.; Straub, A.P. Opportunities for high productivity and selectivity desalination via osmotic distillation with improved membrane design. *J. Membr. Sci.* **2020**, *611*, 118309. [[CrossRef](#)]
13. Essalhi, M.; Kiadeh, N.H.; García-Payo, M.; Khayet, M. 10-Thermo-osmosis. In *Osmosis Engineering*; Hilal, N., Ismail, A.F., Khayet, M., Johnson, D., Eds.; Elsevier: Amsterdam, The Netherlands, 2021; pp. 279–312. [[CrossRef](#)]
14. Skuse, C.; Gallego-Schmid, A.; Azapagic, A.; Gorgojo, P. Can emerging membrane-based desalination technologies replace reverse osmosis? *Desalination* **2021**, *500*, 114844. [[CrossRef](#)]
15. Alsarayreh, A.A.; Al-Obaidi, M.A.; Ruiz-García, A.; Patel, R.; Mujtaba, I.M. Thermodynamic Limitations and Exergy Analysis of Brackish Water Reverse Osmosis Desalination Process. *Membranes* **2022**, *12*, 11. [[CrossRef](#)]
16. Lim, Y.J.; Goh, K.; Kurihara, M.; Wang, R. Seawater desalination by reverse osmosis: Current development and future challenges in membrane fabrication—A review. *J. Membr. Sci.* **2021**, *629*, 119292. [[CrossRef](#)]
17. Zhao, S.; Liao, Z.; Fane, A.; Li, J.; Tang, C.; Zheng, C.; Lin, J.; Kong, L. Engineering antifouling reverse osmosis membranes: A review. *Desalination* **2021**, *499*, 114857. [[CrossRef](#)]
18. Arenas Urrea, S.; Díaz Reyes, F.; Peñate Suárez, B.; de la Fuente Bencomo, J.A. Technical review, evaluation and efficiency of energy recovery devices installed in the Canary Islands desalination plants. *Desalination* **2019**, *450*, 54–63. [[CrossRef](#)]
19. Song, D.; Zhang, Y.; Wang, H.; Jiang, L.; Wang, C.; Wang, S.; Jiang, Z.; Li, H. Demonstration of a piston type integrated high pressure pump-energy recovery device for reverse osmosis desalination system. *Desalination* **2021**, *507*, 115033. [[CrossRef](#)]
20. Zebbar, M.; Messlem, Y.; Gouichiche, A.; Tadjine, M. Super-twisting sliding mode control and robust loop shaping design of RO desalination process powered by PV generator. *Desalination* **2019**, *458*, 122–135. [[CrossRef](#)]
21. Ruiz-García, A.; de la Nuez-Pestana, I. A computational tool for designing BWRO systems with spiral wound modules. *Desalination* **2018**, *426*, 69–77. [[CrossRef](#)]
22. Li, M. A Unified Model-Based Analysis and Optimization of Specific Energy Consumption in BWRO and SWRO. *Ind. Eng. Chem. Res.* **2013**, *52*, 17241–17248. [[CrossRef](#)]
23. Li, M. Optimal plant operation of brackish water reverse osmosis (BWRO) desalination. *Desalination* **2012**, *293*, 61–68. [[CrossRef](#)]
24. Al-hotmani, O.; Al-Obaidi, M.; John, Y.; Patel, R.; Manenti, F.; Mujtaba, I. Minimisation of energy consumption via optimisation of a simple hybrid system of multi effect distillation and permeate reprocessing reverse osmosis processes for seawater desalination. *Comput. Chem. Eng.* **2021**, *148*, 107261. [[CrossRef](#)]
25. AlSawaftah, N.; Abuwatfa, W.; Darwish, N.; Husseini, G. A Comprehensive Review on Membrane Fouling: Mathematical Modelling, Prediction, Diagnosis, and Mitigation. *Water* **2021**, *13*, 1327. [[CrossRef](#)]
26. Niu, C.; Li, X.; Dai, R.; Wang, Z. Artificial intelligence-incorporated membrane fouling prediction for membrane-based processes in the past 20 years: A critical review. *Water Res.* **2022**, *216*, 118299. [[CrossRef](#)]
27. Nthunya, L.N.; Bopape, M.F.; Mahlangu, O.T.; Mamba, B.B.; Van der Bruggen, B.; Quist-Jensen, C.A.; Richards, H. Fouling, performance and cost analysis of membrane-based water desalination technologies: A critical review. *J. Environ. Manag.* **2022**, *301*, 113922. [[CrossRef](#)] [[PubMed](#)]
28. Lu, Y.Y.; Hu, Y.D.; Zhang, X.L.; Wu, L.Y.; Liu, Q.Z. Optimum design of reverse osmosis system under different feed concentration and product specification. *J. Membr. Sci.* **2007**, *287*, 219–229. [[CrossRef](#)]

29. Vince, F.; Marechal, F.; Aoustin, E.; Bréant, P. Multi-objective optimization of RO desalination plants. *Desalination* **2008**, *222*, 96–118. [[CrossRef](#)]
30. Li, M. Minimization of Energy in Reverse Osmosis Water Desalination Using Constrained Nonlinear Optimization. *Ind. Eng. Chem. Res.* **2010**, *49*, 1822–1831. [[CrossRef](#)]
31. Li, M. Reducing specific energy consumption in Reverse Osmosis (RO) water desalination: An analysis from first principles. *Desalination* **2011**, *276*, 128–135. [[CrossRef](#)]
32. Du, Y.; Xie, L.; Wang, Y.; Xu, Y.; Wang, S. Optimization of Reverse Osmosis Networks with Spiral-Wound Modules. *Ind. Eng. Chem. Res.* **2012**, *51*, 11764–11777. [[CrossRef](#)]
33. Du, Y.; Xie, L.; Liu, J.; Wang, Y.; Xu, Y.; Wang, S. Multi-objective optimization of reverse osmosis networks by lexicographic optimization and augmented epsilon constraint method. *Desalination* **2014**, *333*, 66–81. [[CrossRef](#)]
34. Du, Y.; Xie, L.; Liu, Y.; Zhang, S.; Xu, Y. Optimization of reverse osmosis networks with split partial second pass design. *Desalination* **2015**, *365*, 365–380. [[CrossRef](#)]
35. Li, M.; Noh, B. Validation of model-based optimization of brackish water reverse osmosis (BWRO) plant operation. *Desalination* **2012**, *304*, 20–24. [[CrossRef](#)]
36. Jiang, A.; Biegler, L.T.; Wang, J.; Cheng, W.; Ding, Q.; Jiangzhou, S. Optimal operations for large-scale seawater reverse osmosis networks. *J. Membr. Sci.* **2015**, *476*, 508–524. [[CrossRef](#)]
37. Du, Y.; Liu, Y.; Zhang, S.; Xu, Y. Optimization of Seawater Reverse Osmosis Desalination Networks with Permeate Split Design Considering Boron Removal. *Ind. Eng. Chem. Res.* **2016**, *55*, 12860–12879. [[CrossRef](#)]
38. Kotb, H.; Amer, E.; Ibrahim, K. On the optimization of RO (Reverse Osmosis) system arrangements and their operating conditions. *Energy* **2016**, *103*, 127–150. [[CrossRef](#)]
39. Ahunbay, M.G.; Tantekin-Ersolmaz, S.B.; Krantz, W.B. Energy optimization of a multistage reverse osmosis process for seawater desalination. *Desalination* **2018**, *429*, 1–11. [[CrossRef](#)]
40. Alsarayreh, A.A.; Al-Obaidi, M.; Al-Hroub, A.; Patel, R.; Mujtaba, I. Evaluation and minimisation of energy consumption in a medium-scale reverse osmosis brackish water desalination plant. *J. Clean. Prod.* **2020**, *248*, 119220. [[CrossRef](#)]
41. Kim, J.; Park, K.; Hong, S. Optimization of two-stage seawater reverse osmosis membrane processes with practical design aspects for improving energy efficiency. *J. Membr. Sci.* **2020**, *601*, 117889. [[CrossRef](#)]
42. Chu, K.H.; Lim, J.; Kim, S.J.; Jeong, T.U.; Hwang, M.H. Determination of optimal design factors and operating conditions in a large-scale seawater reverse osmosis desalination plant. *J. Clean. Prod.* **2020**, *244*, 118918. [[CrossRef](#)]
43. Chu, K.H.; Oh, B.G.; Kook, S.; Ko, J.; Lim, J.; Kim, H.K.; Chae, K.J.; Hwang, M.H. Operational strategies for brackish water desalination plants in island regions of South Korea. *J. Clean. Prod.* **2021**, *278*, 123540. [[CrossRef](#)]
44. Alnajjar, H.; Tabatabai, A.; Alpatova, A.; Leiknes, T.; Ghaffour, N. Organic fouling control in reverse osmosis (RO) by effective membrane cleaning using saturated CO₂ solution. *Sep. Purif. Technol.* **2021**, *264*, 118410. [[CrossRef](#)]
45. Abushaban, A.; Salinas-Rodriguez, S.G.; Pastorelli, D.; Schippers, J.C.; Mondal, S.; Goueli, S.; Kennedy, M.D. Assessing Pretreatment Effectiveness for Particulate, Organic and Biological Fouling in a Full-Scale SWRO Desalination Plant. *Membranes* **2021**, *11*, 167. [[CrossRef](#)]
46. Yu, W.; Song, D.; Chen, W.; Yang, H. Antiscalants in RO membrane scaling control. *Water Res.* **2020**, *183*, 115985. [[CrossRef](#)] [[PubMed](#)]
47. Chen, Y.; Cohen, Y. Calcium Sulfate and Calcium Carbonate Scaling of Thin-Film Composite Polyamide Reverse Osmosis Membranes with Surface-Tethered Polyacrylic Acid Chains. *Membranes* **2022**, *12*, 1287. [[CrossRef](#)]
48. Guo, Y.; Liu, C.; Liu, H.; Zhang, J.; Li, H.; Zhang, C. Contemporary antibiofouling modifications of reverse osmosis membranes: State-of-the-art insights on mechanisms and strategies. *Chem. Eng. J.* **2022**, *429*, 132400. [[CrossRef](#)]
49. Abushaban, A.; Salinas-Rodriguez, S.G.; Philibert, M.; Le Bouille, L.; Necibi, M.C.; Chehbouni, A. Biofouling potential indicators to assess pretreatment and mitigate biofouling in SWRO membranes: A short review. *Desalination* **2022**, *527*, 115543. [[CrossRef](#)]
50. Ruiz-García, A.; Nuez, I. Long-term performance decline in a brackish water reverse osmosis desalination plant. Predictive model for the water permeability coefficient. *Desalination* **2016**, *397*, 101–107. [[CrossRef](#)]
51. Park, J.; Jeong, K.; Baek, S.; Park, S.; Ligaray, M.; Chong, T.H.; Cho, K.H. Modeling of NF/RO membrane fouling and flux decline using real-time observations. *J. Membr. Sci.* **2019**, *576*, 66–77. [[CrossRef](#)]
52. Ruiz-García, A.; Ruiz-Saavedra, E. 80,000 h operational experience and performance analysis of a brackish water reverse osmosis desalination plant. Assessment of membrane replacement cost. *Desalination* **2015**, *375*, 81–88. [[CrossRef](#)]
53. Wilf, M.; Klinko, K. Performance of commercial seawater membranes. *Desalination* **1994**, *96*, 465–478. [[CrossRef](#)]
54. Tolba, A.; Mohamed, R. Performance and characteristics of reverse osmosis membranes. In Proceedings of the 4th International Water Technology Conference, Alexandria, Egypt, 1999; pp. 171–181. Available online: <https://citeseerx.ist.psu.edu/document?repid=rep1&type=pdf&doi=70265438f06c545a65b3b50b1461d3edb39279d6> (accessed on 2 July 2023).
55. Abbas, A.; Al-Bastaki, N. Performance decline in brackish water FilmTec spiral wound RO membranes. *Desalination* **2001**, *136*, 281–286. [[CrossRef](#)]
56. Belkacem, M.; Bekhti, S.; Bensadok, K. Groundwater treatment by reverse osmosis. *Desalination* **2007**, *206*, 100–106. [[CrossRef](#)]
57. Sassi, K.M.; Mujtaba, I.M. Optimal design and operation of reverse osmosis desalination process with membrane fouling. *Chem. Eng. J.* **2011**, *171*, 582–593. [[CrossRef](#)]

58. Park, P.K.; Lee, S.; Cho, J.S.; Kim, J.H. Full-scale simulation of seawater reverse osmosis desalination processes for boron removal: Effect of membrane fouling. *Water Res.* **2012**, *46*, 3796–3804. [[CrossRef](#)]
59. Ang, W.; Nordin, D.; Mohammad, A.; Benamor, A.; Hilal, N. Effect of membrane performance including fouling on cost optimization in brackish water desalination process. *Chem. Eng. Res. Des.* **2017**, *117*, 401–413. [[CrossRef](#)]
60. Kim, J.; Hong, S. Optimizing seawater reverse osmosis with internally staged design to improve product water quality and energy efficiency. *J. Membr. Sci.* **2018**, *568*, 76–86. [[CrossRef](#)]
61. Lee, Y.G.; Kim, S.; Shin, J.; Rho, H.; Kim, Y.M.; Cho, K.H.; Eom, H.; Oh, S.E.; Cho, J.; Chon, K. Sequential effects of cleaning protocols on desorption of reverse osmosis membrane foulants: Autopsy results from a full-scale desalination plant. *Desalination* **2021**, *500*, 114830. [[CrossRef](#)]
62. Jeong, S.; Naidu, G.; Vollprecht, R.; Leiknes, T.; Vigneswaran, S. In-depth analyses of organic matters in a full-scale seawater desalination plant and an autopsy of reverse osmosis membrane. *Sep. Purif. Technol.* **2016**, *162*, 171–179. [[CrossRef](#)]
63. Chu, H.; Ma, J.; Liu, X.; Wang, F.; Zhou, X.; Zhang, Y.; Li, E.; Zhang, X. Spatial evolution of membrane fouling along a multi-stage integrated membrane system: A pilot study for steel industry brine recycling. *Desalination* **2022**, *527*, 115566. [[CrossRef](#)]
64. Ruiz-García, A.; Nuez, I. Simulation-based assessment of safe operating windows and optimization in full-scale seawater reverse osmosis systems. *Desalination* **2022**, *533*, 115768. [[CrossRef](#)]
65. Zubair, M.M.; Saleem, H.; Zaidi, S.J. Recent progress in reverse osmosis modeling: An overview. *Desalination* **2023**, *564*, 116705. [[CrossRef](#)]
66. Ruiz-García, A.; Nuez, I. A time-dependent model of pressure drop in reverse osmosis spiral wound membrane modules. *IFAC-PapersOnLine* **2021**, *54*, 158–163. [[CrossRef](#)]
67. Geraldes, V.; Pereira, N.E.; de Pinho, M.N. Simulation and Optimization of Medium-Sized Seawater Reverse Osmosis Processes with Spiral-Wound Modules. *Ind. Eng. Chem. Res.* **2005**, *44*, 1897–1905. [[CrossRef](#)]
68. Schock, G.; Miquel, A. Mass transfer and pressure loss in spiral wound modules. *Desalination* **1987**, *64*, 339–352. [[CrossRef](#)]
69. Duan, R.; Lv, X.; Yan, W.; Zhou, Y.; Gao, C. Fabrication of high boron removal reverse osmosis membrane with broad industrial application prospect by introducing sulfonate groups through a polyvinyl alcohol coating. *J. Membr. Sci.* **2022**, *664*, 121079. [[CrossRef](#)]
70. Li, C.; Zhao, Y.; Lai, G.S.; Wang, R. Fabrication of fluorinated polyamide seawater reverse osmosis membrane with enhanced boron removal. *J. Membr. Sci.* **2022**, *662*, 121009. [[CrossRef](#)]
71. Boussouga, Y.A.; Richards, B.S.; Schäfer, A.I. Renewable energy powered membrane technology: System resilience under solar irradiance fluctuations during the treatment of fluoride-rich natural waters by different nanofiltration/reverse osmosis membranes. *J. Membr. Sci.* **2021**, *617*, 118452. [[CrossRef](#)]

Disclaimer/Publisher’s Note: The statements, opinions and data contained in all publications are solely those of the individual author(s) and contributor(s) and not of MDPI and/or the editor(s). MDPI and/or the editor(s) disclaim responsibility for any injury to people or property resulting from any ideas, methods, instructions or products referred to in the content.